Chinese Chemical Letters 37 (2026) 111959

Contents lists available at ScienceDirect

Chinese Chemical Letters

journal homepage: www.elsevier.com/locate/cclet

4D printing of reprocessable thiocyanate covalent adaptable networks with reconfigurable shape memory ability

Ting Xu, Kexiang Chen, Zhiyuan He, Chuanzhen Zhang, Xiaoyu Li, Ziyan Zhang, Wenbo Fan, Zhishen Ge, Chenhui Cui*, Yanfeng Zhang*

School of Chemistry, State Key Laboratory of Fluorine & Nitrogen Chemicals, Institute of New Concept Sensors and Molecular Materials (INCSMM), Engineering Research Center of Energy Storage Materials and Devices, Ministry of Education, Xi'an Key Laboratory of Sustainable Polymer Materials, Xi'an Jiaotong University, Xi'an 710049, China

ARTICLE INFO

Article history:
Received 13 June 2025
Revised 6 October 2025
Accepted 13 October 2025
Available online 15 October 2025

Keywords:
4D Printing
Dynamic thiocyanate ester bonds
Covalent adaptable networks
Cyanate ester resin
Shape memory

ABSTRACT

Shape memory polymers used in 4D printing only had one permanent shape after molding, which limited their applications in requiring multiple reconstructions and multifunctional shapes. Furthermore, the inherent stability of the triazine ring structure within cyanate ester (CE) crosslinked networks after molding posed significant challenges for both recycling, repairing, and degradation of resin. To address these obstacles, dynamic thiocyanate ester (TCE) bonds and photocurable group were incorporated into CE, obtaining the recyclable and 3D printable CE covalent adaptable networks (CANs), denoted as PTCE1.5. This material exhibits a Young's modulus of 810 MPa and a tensile strength of 50.8 MPa. Notably, damaged printed PTCE1.5 objects can be readily repaired through reprinting and interface rejoining by thermal treatment. Leveraging the solid-state plasticity, PTCE1.5 also demonstrated attractive shape memory ability and permanent shape reconfigurability, enabling its reconfigurable 4D printing. The printed PTCE1.5 hinges and a main body were assembled into a deployable and retractable satellite model, validating its potential application as a controllable component in the aerospace field. Moreover, printed PTCE1.5 can be fully degraded into thiol-modified intermediate products. Overall, this material not only enriches the application range of CE resin, but also provides a reliable approach to addressing environmental issue.

© 2025 Published by Elsevier B.V. on behalf of Chinese Chemical Society and Institute of Materia Medica, Chinese Academy of Medical Sciences.

Four-dimensional (4D) printing represented an advanced additive manufacturing technology that featured high-precision and complex structural fabrication. Furthermore, by incorporating the fourth dimension "time" into three-dimensional (3D) printing [1–3], structures obtained through 4D printing technology could be dynamically deformed or functionally transformed under specific external stimuli, including heat [4], light [5], electricity [6], pH [7], moisture [8], magnetic fields [9]. Owing to its stimuli-triggered characteristic, 4D printing has demonstrated remarkable potential in biomedical [5], architecture [10], robotics [4,11], textiles [12], and others. Typically, materials utilized in 4D printing included shape-memory polymers (SMPs), shape-memory alloys [13], hydrogels, smart ceramics [14]. Among them, SMPs showed great potential for application in many fields due to their low cost, lightweight, ease of processing, large deformation, and excellent biocompatibility [15–20]. For instance, Feng *et al.* reported 4D printing of SMPs and achieved reversibly photoswitchable, spatial, and remote control [21]. However, most SMPs used in 4D printing were thermosetting materials, which only have one permanent shape after printing [22]. This significantly hindered their potential in applications requiring multiple reconstructions and multifunctional shapes. Hence, it was on demand to develop a permanent shape reconfigurable, recyclable, and chemically degradable material for 4D printing.

Recently, introducing dynamic covalent bonds into SMPs could endow them with reprocessing and recycling capabilities similar to thermoplastic materials [23]. Cyanate ester (CE) resin was a type of thermosetting resin with shape memory, which was synthesized through the cyclotrimerization reaction [24]. Due to its excellent mechanical performance, low moisture absorption, thermal stability, and low dielectric property, CE resin was well-suited for various applications such as high-performance printed circuit boards, and antenna radomes [25]. However, the permanent triazine ring containing network that endowed CE with superior performance simultaneously made it difficult to recycle or degrade after curing. This recyclability limitation motivated recent investigations into

* Corresponding authors.
E-mail addresses: cuichenhui@xjtu.edu.cn (C. Cui), yanfengzhang@mail.xjtu.edu.cn (Y. Zhang).

https://doi.org/10.1016/j.cclet.2025.111959
1001-8417/© 2025 Published by Elsevier B.V. on behalf of Chinese Chemical Society and Institute of Materia Medica, Chinese Academy of Medical Sciences.

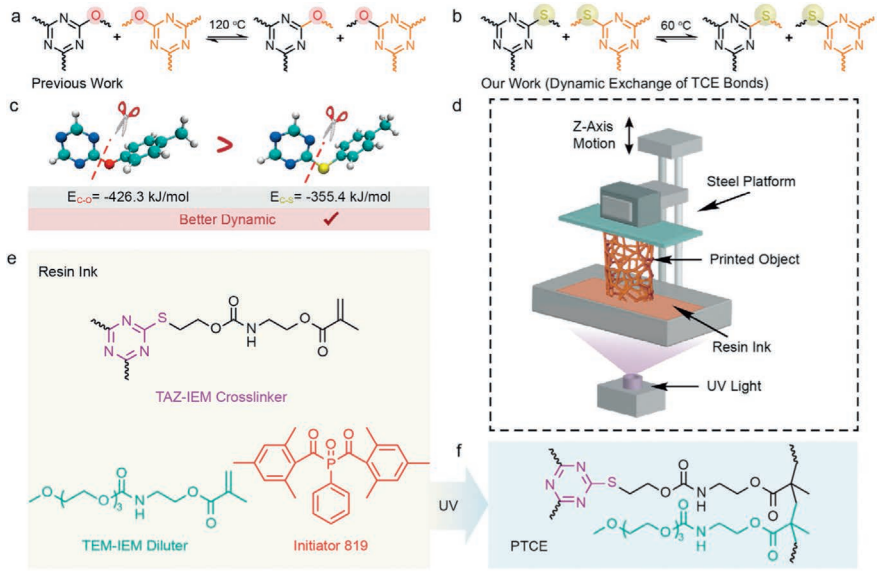


Fig. 1. Schematic illustration of the printing process and ink components for the 4D printing of the PTCE materials. (a) Previously developed dynamic cyanate ester bonds [28]. (b) Calculation of bond dissociation energies from DFT. (c) Dynamic exchange reaction of TCE bonds. (d) Composition of PTCE precursor solution for DLP printing. (e) Schematic diagram of UV curing mechanism. (f) Polymer structure of the PTCE.

CE-based covalent adaptable networks (CANs), which exhibited the ability to organize the networks of recycle, repair and reprocess by introducing dynamic covalent bonds. Building on retrosynthetic analysis [26], Zhang *et al.* reported a novel approach to impart recyclability to CE through dynamic nucleophilic aromatic substitution [27,28]. However, the substantial incorporation of catalysts (10 mol%) aimed at enhancing the reprocessing of material led to a significant reduction in its mechanical strength (~2.6 MPa). Therefore, developing covalent bonds with high dynamicity was necessary for the application of CE in 4D printing.

The main advantage of 4D printing lied in its ability to fabricate complex and precise components. Currently, the molding and processing of CE resin primarily relied on traditional methods such as compression molding, injection molding, and lamination. However, these techniques were constrained by low precision and limited design, making it challenging to meet the demands for fabricating complex and precise components in fields such as aerospace and microelectronics. Nevertheless, the development of CE resin for printing remained at the exploratory stage. Current research efforts primarily focused on two approaches. One was adjusting its rheological property to make the prepolymer of CE resin suitable for direct ink writing (DIW) printing. Zhao *et al.* studied the use of polytetrafluoroethylene micropowder to regulate the rheological properties of ink for printing of CE [29]. Similarly, Lewicki *et al.* formulated CE ink by adding silica nanoparticles and fabricated complex components through DIW [30]. However, this additive manufacturing approach exhibited constrained dimensional precision due to the inherent material characteristics and the extrusion mechanism employed. The other method was to mix the CE monomers with photocurable resin, which played a setting role during the DLP printing process. Some researchers dissolved acrylate in CE monomers, in which the carbon–carbon double bonds from acrylate were cured by radical polymerization, followed by postprinting thermal treatment to convert three cyanate groups into a triazine ring structure [31]. The drawback of this method was that the high temperature treatment process after printing required the photosensitive resin to have a high glass transition temperature to maintain its original shape. Therefore, to accelerate and simplify the molding process of CE resin, it was valuable to develop a forming technology of high-precision printable CE resin.

Recently, our research group developed thiocarbamate bonds, which significantly enhanced dynamic behavior compared to carbamate bonds [32–34]. According to valence bond theory [35], the 2p orbitals of an oxygen atom exhibited energy level matching with the 2p orbitals of a carbon atom, enabling stable orbital overlap. In contrast, the 3p orbitals of a sulfur atom displayed energy level discrepancies with 2p orbitals, resulting in poor orbital overlap. This made the C-S bond more prone to distortion, ultimately leading to a lower bond energy. Therefore, compared to the C–O bond, C-S bond featured a better dynamic exchange performance. In this study, we adopted this strategy to synthesize the dynamic thiocyanate ester (TCE) bond. Compared with the cyanate ester bond (426.3 kJ/mol) (Fig. 1a), the lower bond energy of TCE (355.4 kJ/mol) endowed it with superior dynamic properties (Figs. 1b and c). Specifically, polythiocyanate ester (PTCE) was prepared using a DLP printer (405 nm UV mode), and the printing ink contained of TCE bond-containing two-step synthetic dynamic crosslinker (TAZ-IEM), reactive diluent (TEM-IEM), and initiator 819 (Figs. 1d-f). The methacrylate groups were converted layer by layer into crosslinked polymers of predetermined structure by free radical polymerization. $PTCE_{1.5}$ material exhibited high mechanical performance and chemical stability, while the dynamic exchange reaction of TCE bonds gave it excellent remodelability and reconfigurable 4D printing. By printing the deployable and contractile satellite model, the potential application of $PTCE_{1.5}$ as a controllable component in the aerospace field was validated. Furthermore, the printed $PTCE_{1.5}$ can be degraded into thiol-modified intermediate products.

First, we investigated the dynamic properties of covalent bonds using density functional theory (DFT). When the oxygen atom in cyanate ester was replaced by a sulfur atom with a larger atomic radius, the C–S bond (355.4 kJ/mol) exhibited significantly lower bond energy and higher propensity for bond dissociation compared to the C–O bond (426.3 kJ/mol). Based on this, the dynamic properties of the TCE bond were further systematically explored.

A dynamic exchange study of the model compounds was performed to verify their active dynamic behavior. We first used 2,4,6-tris(*p*-toluenethio)-1,3,5-triazine (**A**) and 2,4,6-tris(benzylthio)-1,3,5-triazine (**B**) as model compounds to study the reversibility of the nucleophilic aromatic substitution between thiocyanates. In

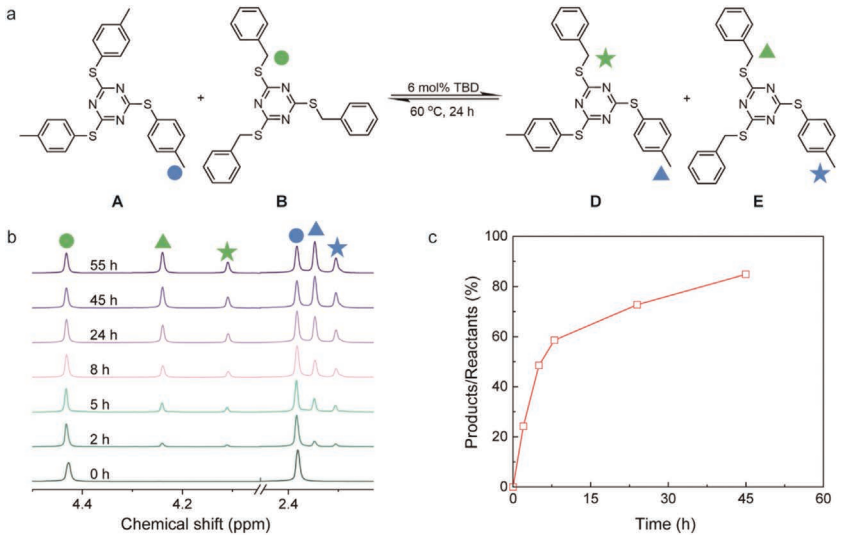


Fig. 2. Verification of the dynamic behavior of TCE bonds. (a) Exchange reaction between **A** and **B**. (b) Reaction process of ^{1}H NMR spectra at 60 °C for 55 h. (c) Extent of the reaction changes over time.

the absence of any catalyst, no exchange reaction occurred in the system at 60 °C (Fig. S8 in Supporting information). Conversely, when 6 mol% triazabicyclodecene (TBD) of compound **A** was added, the model compounds system resulted in the formation of two distinct compounds, 2,4-bis(*p*-toluenethio)-6-benzylthio-1,3,5-triazine (**D**) and 2-*p*-toluenethio-4,6-bis(benzylthio)-1,3,5-triazine (**E**) (Fig. 2a). The new two peaks at 4.24 and 4.11 ppm were attributed to the methylene protons of the benzylthio groups, while the peaks at 2.34 and 2.30 ppm were assigned to the methyl protons of the *p*-toluenethiol groups (Fig. 2b and Fig. S9 in Supporting information). This demonstrated that the organic base TBD can promote the dynamic exchange of TCE bonds. We monitored the reaction progress at 60 °C over various time intervals, and the results indicated that equilibrium was reached after 45 h (Fig. 2c). Collectively, these results revealed reversibility of the TCE bonds, which allowed us to further prepare and investigate dynamic behaviors of CANs containing TCE bonds.

Next, we investigated the dynamic exchange behavior between different steric thiocyanates and thiols by conducting exchange reactions of butanethiol with compounds **A** and **B**, respectively (Fig. S10 in Supporting information). In the mixture A system (Scheme S7 in Supporting information), the emergence of characteristic signals at 2.88–2.96 ppm during the exchange reaction confirmed the formation of new compound **F**, while the peak observed at 2.80–2.67 ppm indicated the generation of compound **E**. The distinct peak at 2.26 ppm was attributed to the liberated *p*-toluenethiol through substitution. Concurrently, in the mixture B system (Scheme S7), the appearance of a triplet at 3.13 ppm demonstrated the formation of new compound **G**, with the resonance at 3.76 ppm corresponding to the benzyl mercaptan. However, under the same conditions, compound **C** did not undergo an exchange reaction with *n*-butanol, indicating that C-S bonds exhibit higher exchange reactivity than C–O bonds (Fig. S11 in Supporting information). The reaction progress was quantitatively analyzed by integrating the methyl protons of the released small molecule *p*-toluenethiol and the methylene protons of benzyl mercaptan. Notably, compared to compound **A** featuring *p*-toluenethio, compound **B** with benzyl mercaptan exhibited a faster exchange rate, achieving a 3.4-fold reaction rate of compound **A** after 64 min. This phenomenon could be attributed to the heightened electron density of the sulfur atom in compound **A**, which was induced by the conjugation effect of the phenyl ring. This increased electron density stabilized the bond between the sulfur atom and the electron-deficient carbon atom of the triazine ring, thereby significantly enhancing the bond energy. In contrast, the methylene group in compound **B** exhibited an isolating effect, which diminished its stability, resulting in superior dynamic properties. These results revealed the dynamic behavior of TCE bonds and provided a rationale for selecting alkylthio cyanate monomers for the subsequent investigation of CANs based on dynamic.

Following the validation of the dynamic bond behavior, we next investigated the part of the photocurable crosslinker TAZ-IEM containing dynamic TCE bonds. This crosslinking agent was synthesized in two steps (Fig. 3a). Cyanuric chloride was first reacted with 2-mercaptoethanol, introducing dynamic TCE bonds while retaining terminal hydroxyl groups, which can further serve as reactive sites. In the second step, 2-isocyanatoethyl methacrylate (IEM) was added, and the nucleophilic addition reaction occurred between the hydroxyl groups and the isocyanate groups, yielding the trifunctional crosslinking agent. The structure was confirmed by proton nuclear magnetic resonance (^{1}H NMR) and Fourier-transfer infrared (FTIR) spectroscopic analyses (Figs. S5 and S12 in Supporting information). Rheological behavior, especially viscosity, plays a crucial role in determining whether precursor inks are suitable for DLP printing. Along with separating the cured structure from the curing interface, the ink must refill the gap between the curing structure and the curing interface to create a new liquid layer for the next curing layer to accumulate [36]. As a result, inks with high viscosity and poor fluidity can slow down the printing process and lead to defects and failures. TEM-IEM monomer was added to TAZ-IEM as a reaction diluent to regulate the viscosity of the precursor ink. It was found that as the mass ratio of TEM-IEM increased from 0 wt% to 60 wt%, the viscosity of TAZ-TEM ink decreased from 2173.7 Pa s to 0.2 Pa s (Fig. 3b). Based on previous reports, the ink with a viscosity lower than 3.0 Pa s is more suitable for DLP printing [37]. Therefore, we chose the precursor ink with >50 wt% TEM-IEM content for printing. The addition of the reactive diluent TEM-IEM reduced the viscosity of the printing ink, but also simultaneously decreased the content of the crosslinker TAZ-IEM, which provided dynamic exchange performance and increased the crosslink density of the network. The cured ink containing 50 wt% TEM-IEM exhibited higher Young's modulus and tensile strength compared to the component with 60 wt% TEM-IEM (Fig. 3c and Table S1 in Supporting information). The results showed that the exis-

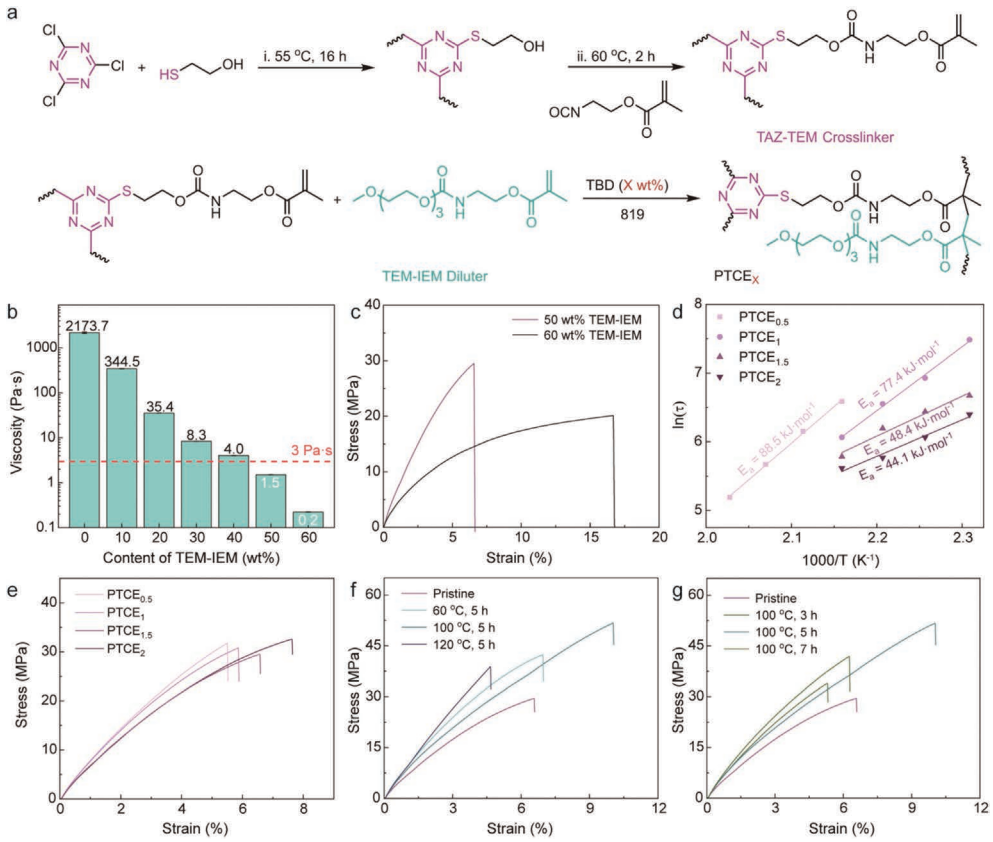


Fig. 3. Design of printing ink and mechanical properties of PTCE. (a) Synthesis of crosslinker agent and active diluent. (b) Viscosity of different TEM-IEM content systems. (c) Mechanical properties of different TEM-IEM content systems. (d, e) Apparent activation energy and mechanical properties of different TBD content systems. (f) Stress-strain curves of PTCE1.5 treated at different annealing temperatures. (g) Stress-strain curves of PTCE1.5 treated at different annealing times.

tence of chemical structure with high crosslinking degree could enhance the mechanical properties of the materials. Therefore, we selected the composition with 50 wt% TEM-IEM content (designated as PTCE) for investigation.

Organic base TBD was added to the PTCE$_X$ (X denoted the percentage value of TBD relative to monomer mass) samples as catalyst, which could trigger the dynamic exchange of TCE bonds in the polymer networks under heat treatment. We performed stress relaxation tests at different temperatures to explore the effect of TBD catalyst content (0.5 wt%, 1 wt%, 1.5 wt%, 2 wt%) on the kinetics of TCE bonds' exchange (Fig. S13 in Supporting information). As the catalyst content increased from 0.5 wt% to 2 wt%, the relaxation time of PTCE$_X$ at 190 °C showed a significant decrease from 725 s to 275 s, corresponding to 38 % of the initial value. The apparent activation energy of PTCE$_X$ was calculated using the Arrhenius equation of 88.5 kJ/mol, which decreased to 44.1 kJ/mol as the catalyst content increased to 2 wt% (Fig. 3d). The results showed that TBD could greatly accelerate the exchange rate of TCE bonds, and further increase the network topology rearrangement rate. Moreover, we verified the effect of TBD content on the mechanical and thermal properties of PTCE$_X$ samples. The uniaxial tension tests of the PTCE$_X$ samples with different TBD content showed the alike stress-strain curves with failure strain of >5 % and fracture strength of >29 MPa, revealing that the TBD content had no significant effect on the mechanical behavior of the PTCE$_X$ samples (Fig. 3e and Table S2 in Supporting information). Besides, the PTCE$_X$ samples with different TBD content exhibited similar glass transition temperatures (T_g) of ~82 °C by dynamic mechanical analysis (DMA), which was consistent with the mechanical results (Fig. S14 in Supporting information). Thermogravimetry analysis (TGA) results showed that the thermal decomposition temperature ($T_{d,5\%}$) decreased from 230 °C to 201 °C as the TBD content was increased from 0.5 wt% to 2 wt% (Fig. S15 in Supporting information). The accelerated thermal decomposition could be attributed to the fact that the increased TBD provided more active sites, facilitating the cleavage and recombination of bonds, and weakening the network structure of the material. Based on the above comprehensive considerations of dynamic behaviors, mechanical properties and thermal stabilities, we set TBD content as 1.5 wt% to further study.

Considering the combined effects of ink viscosity, TBD content on material properties, and the mechanical performance of cured components, the printing ink with TEM-IEM content of 50 wt% and TBD concentration of 1.5 wt% was selected for study. To confirm the formation of the crosslinked network, swelling experiments were conducted by immersing samples in seven solvents at room temperature. PTCE$_{1.5}$ exhibited swelling ratios ranging from 1 % to 40 %, and the gel fractions were above 87 %, confirming the formation of a highly crosslinked network (Fig. S16 in Supporting information).

For photocurable 3D printing materials, unreacted C=C bonds and internal stress generated during printing contribute to the degradation of their mechanical properties. Annealing treatment can promote further crosslinking of the C=C bonds while simultaneously relieving internal stress, enhancing overall mechanical properties. To explore an appropriate annealing treatment condition, samples were isothermally treated at 60, 100, and 120 °C for a fixed annealing time of 5 h, with subsequent evaluation of mechanical properties (Fig. 3f). It was observed that the tensile strength increased to 50.8 MPa and breaking elongation reached 10.0 % with the increase in thermal treatment temperature except 120 °C (Table S3 in Supporting information), which may be attributed to the further reaction of C=C bonds (Fig. S17 in Supporting information)

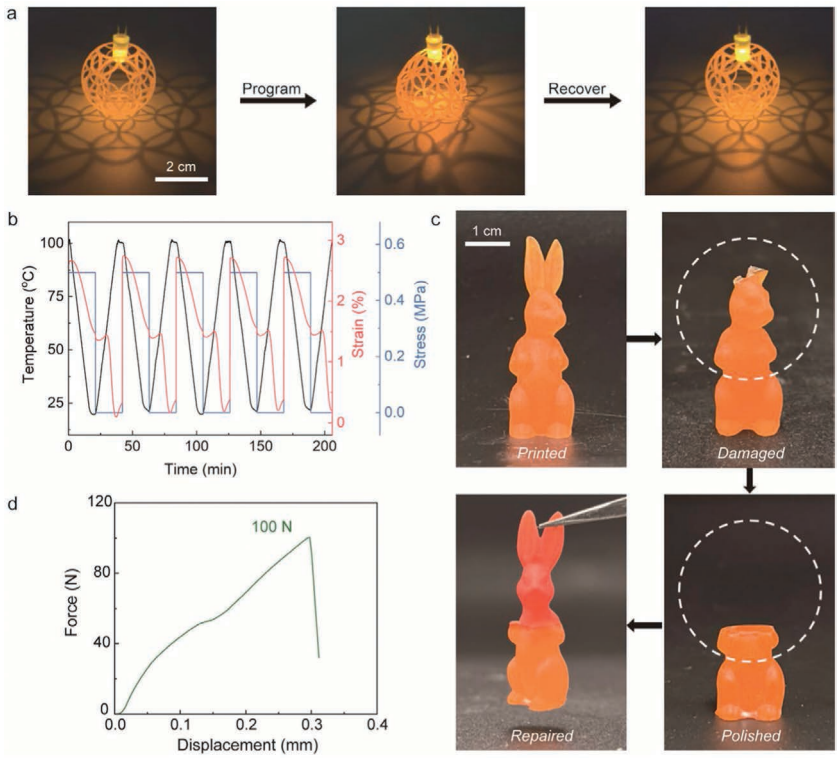


Fig. 4. Shape memory and repairing of PTCE1.5. (a) Shape memory photographs of a stereoscopic projection sample. (b) Shape memory curves for 5 cycles of PTCE1.5 obtained by DMA. (c) Photographs of repairing a damaged printed rabbit. (d) Interfacial force of PTCE1.5 *via* section printing.

and the relief of internal stress by reorganization of dynamic networks. However, annealing at high temperatures (120 °C) caused a small amount of thermal decomposition of the materials, resulting in a deterioration of the tensile strength to 37.9 MPa. Subsequently, the mechanical properties were characterized at a fixed temperature of 100 °C for different annealing times (3, 5, and 7 h) (Fig. 3g). The results showed that with the increase in annealing treatment time, the mechanical properties of the samples improved (Table S4 in Supporting information) due to additional crosslinking and rearrangement of the polymer network (Fig. S18 in Supporting information). However, an excessively long annealing treatment time (7 h) also decreased tensile strength to 44.9 MPa. Based on the above results, the optimal annealing treatment conditions were determined to be 100 °C for 5 h.

Compared with traditional casting, the primary advantage of 3D printing lies in its ability to create more complex and precise structures. The Oriental Pearl Tower printed by $PTCE_{1.5}$ perfectly restored the appearance of the printed model, showing the high printing fidelity at a macro level (Fig. S19 in Supporting information). The SEM image of the printed Oriental Pearl Tower clearly indicated that during the photo-curing process, the sample was composed of layered stacking structures. Furthermore, $PTCE_{1.5}$ was found to attain a printing resolution of up to ~136 μm using a DLP printer (Fig. S20 in Supporting information). The realization of high fidelity 3D printing benefited from the appropriate viscosity of the resin.

In the field of 4D printing, SMPs with crosslinked networks play a crucial role. To illustrate the shape memory performance, we printed a stereoscopic projection sample with $PTCE_{1.5}$. The structure of the sample gradually spontaneously recovered from the twisted state to the initial state within 15 s at a temperature of 100 °C, showing rapid recovery ability (Fig. 4a and Movie S1 in Supporting information). The 5 cycles memory process of DMA showed that the shape recovery (R_r) of $PTCE_{1.5}$ was 88.3 %, and no significant strain displacement was detected due to the stability of the crosslinked network (Fig. 4b). The shape fixity ratio of $PTCE_{1.5}$ measured 54 %. The relatively low fixity rate may be attributed to insufficient network density from high monofunctional diluent content and lack of phase-transition-driven fixation mechanisms. The $PTCE_{1.5}$ printed objects obtained by DLP technology exhibited high printing resolution and excellent shape memory properties.

3D printed objects may be damaged or broken during operation, making it difficult to repair for thermosetting resins containing covalent crosslinked networks. $PTCE_{1.5}$ featured great repairing ability due to the presence of dynamic TCE bonds, making it easy to self-repair damaged parts and be further reused. As shown in Fig. 4c, to repair the damaged head of the printed rabbit, we polished the damaged area and reprinted a new head on the polished interface. After heating at 140 °C for 3 h, the TCE bonds exchange reaction between the interfaces was promoted by thermal activation, resulting in the robust bonding of the newly printed section. Furthermore, tensile testing showed that the maximum load-bearing capacity of the interfacial region reached 104 N, achieving effective repair of the damaged model (Fig. 4d).

Solar wings are an important application of shape-adaptable structures in the aerospace field. Herein, we printed $PTCE_{1.5}$ hinges and a main body were assembled into a deployable and retractable satellite model, which changed its permanent shape through solid-state plasticity to achieve both deployment and contraction functions. Once the bent hinges were reheated to 100 °C, they could return to their original open state (Fig. S21a in Supporting information). Most importantly, the hinges were bent into a temporary shape at 140 °C and maintained for 10 h, during which the network topology undergoes adaptable rearrangement, resulting in a changed permanent shape. Subsequently, the hinges were capable of achieving a retraction function (Fig. S21b and Movie S2 in Supporting information). In space, all forms of resources were particularly precious. If combined with solar panels, thermal energy

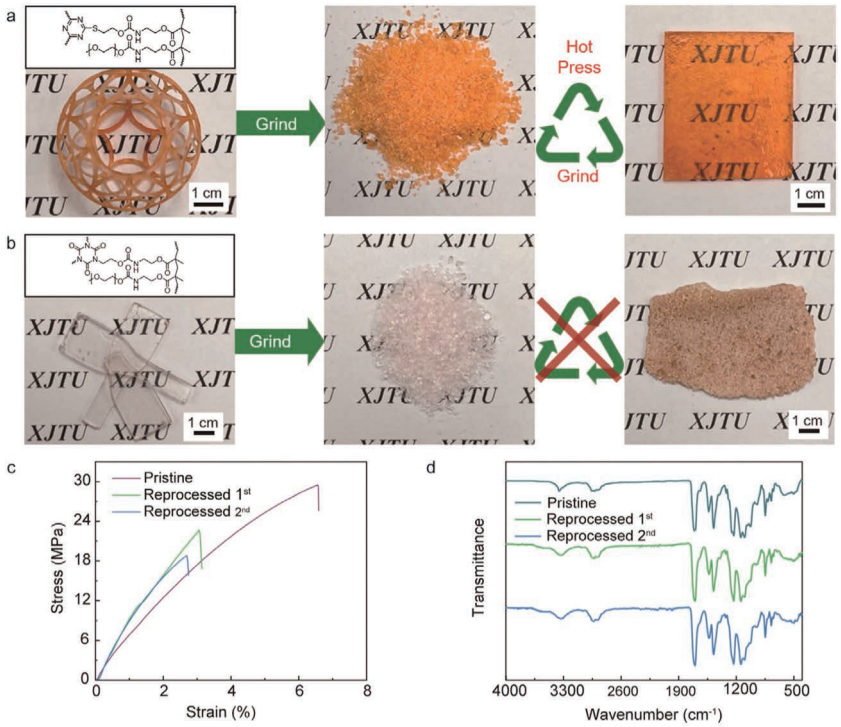


Fig. 5. Reprocessing recycling and chemical degradation of PTCE1.5. (a) Reprocessing regeneration process of PTCE1.5 from powder to bulk. (b) Reprocessing regeneration process of PTT1.5. (c) Stress-strain curves of the pristine samples and the two generations of reprocessing of PTCE1.5 samples. (d) FTIR spectra of the two generations of reprocessing of PTCE1.5 samples.

can be effectively converted into kinetic energy, thereby reducing power transmission and conserving valuable electrical resources.

Besides, the dynamic behavior of TCE bonds endowed the $PTCE_{1.5}$ with reprocessability. The printed samples were ground into powder and hot pressed at 140 °C under 3 MPa pressure for 4 h, enabling two cycles of sample recycling (Fig. 5a). Compared to $PTT_{1.5}$ without dynamic TCE bonds, recycling could not be achieved under the same hot-pressing conditions (Fig. 5b). Tensile testing was employed to characterize the mechanical properties of the recycled materials. As shown in Fig. 5c, after two recycling cycles, the Young's modulus increased from 683 MPa to 956 MPa due to the high pressure and crosslinking of residual double bonds (Fig. S22 in Supporting information), making the network denser. (Table S5 in Supporting information). The tensile strength and breaking elongation decreased to 20 MPa and 2.6 % respectively, which were attributed to a small amount of thermal decomposition caused by high temperature treatment. The FTIR spectra of the original and recycled $PTCE_{1.5}$ were identical, indicating that its chemical composition was the same as that of the original sample and exhibited good reproducibility, even after two cycles of hot pressing (Fig. 5d). Due to a highly covalent crosslinked network, $PTCE_{1.5}$ only swelled rather than dissolved in various solvents. To achieve degradation of the thermosetting resin, we mixed PTCE with TBD in 1,8-dimercapto-3,6-dioxaoctane (DODT) to evaluate the chemical degradability. The newly added DODT underwent an exchange reaction with the CANs under the catalysis of TBD, converting $PTCE_{1.5}$ into thiol-modified intermedia products that dissolved in the solvent after 48 h (Fig. S23a in Supporting information). In contrast, $PTT_{1.5}$ without dynamic TCE bonds could not undergo chemical degradation under the same conditions (Fig. S23b in Supporting information). The above results proved $PTCE_{1.5}$ containing dynamic TCE bonds have excellent reprocessing recycling and chemical degradation ability.

In summary, we reported a kind of photocuring printable CE designated as $PTCE_{1.5}$ through strategic incorporation of dynamic thiocyanate bonds. The rapid exchange ability of TCE bonds was effectively confirmed through model compounds, and the benzylthio-triazine derivative exhibited superior dynamic behavior compared to the *p*-toluenethio-triazine derivative due to its low conjugation. By optimizing the monomer ratio, catalyst concentration, and annealing process, the resin with excellent mechanical properties, reprocessing, and chemical degradation was prepared. The solid-state plasticity imparted by TCE bonds enabled the resin to exhibit reconfigurable shape memory, positioning the CANs for aerospace adaptable components. Overall, this material not only greatly enriches the application range of CE resin, but also provides a reliable approach to addressing environmental pollution and energy crises.

Declaration of competing interest

The authors declare that they have no known competing financial interests or personal relationships that could have appeared to influence the work reported in this paper.

CRediT authorship contribution statement

Ting Xu: Writing – original draft, Investigation, Formal analysis. **Kexiang Chen:** Data curation. **Zhiyuan He:** Investigation. **Chuanzhen Zhang:** Resources. **Xiaoyu Li:** Formal analysis. **Ziyan Zhang:** Visualization. **Wenbo Fan:** Data curation. **Zhishen Ge:** Writing – review & editing. **Chenhui Cui:** Writing – review & editing, Conceptualization. **Yanfeng Zhang:** Writing – review & editing, Funding acquisition, Conceptualization.

Acknowledgments

This work was supported by the National Natural Science Foundation of China (Nos. 52473080, 52403167 and 52173079), the Fundamental Research Funds for the Central Universities

(Nos. xtr052023001 and xzy012023037), the Postdoctoral Research Project of Shaanxi Province (No. 2024BSHSDZZ054), the Shaanxi Laboratory of Advanced Materials (No. 2024ZY-JCYJ-04-12). The authors gratefully thank the Instrument Analysis Center of Xi'an Jiaotong University for assistance with NMR analysis.

Supplementary materials

Supplementary material associated with this article can be found, in the online version, at doi:10.1016/j.cclet.2025.111959.

References

[1] J. Yang, Y.X. Cheng, X. Gong, et al., Chin. Chem. Lett. 33 (2022) 2231–2242.
[2] A.K. Zhang, F. Wang, L. Chen, et al., Chin. Chem. Lett. 32 (2021) 2923–2932.
[3] M.N. He, Y. Zhao, Y.Q. Liu, D.C. Wei, Chin. Chem. Lett. 31 (2020) 826–830.
[4] J. Zhang, M.K. Xu, N. Zhang, et al., Small 20 (2024) 2406358.
[5] Y.Y. Li, J.Q. You, H.X. Lv, et al., Chem. Eng. J. 489 (2024) 151205.
[6] D. Grinberg, S. Siddique, M.Q. Le, et al., J. Polym. Sci. B 57 (2019) 109–115.
[7] Y.L. Hu, Z.Y. Wang, D.D. Jin, et al., Adv. Funct. Mater. 30 (2020) 1907377.
[8] I. Choi, S. Jang, S. Jung, et al., Mater. Horizons 10 (2023) 3668–3679.
[9] C.Y. Deng, J.T. Qu, J.H. Dong, et al., Chem. Eng. J. 494 (2024) 152992.
[10] R. El-Dabaa, I. Salem, Open House Int. 46 (2021) 376–390.
[11] Y. Wang, H.X. Xuan, L.Z. Zhang, et al., Adv. Mater. 36 (2024) 2313761.
[12] M.C. Biswas, S. Chakraborty, A. Bhattacharjee, Z. Mohammed, Adv. Funct. Mater. 31 (2021) 2100257.
[13] Y.K. Zhang, L.Y. Xu, L. Zhao, et al., J. Mater. Sci. Technol. 167 (2023) 14–26.
[14] R. Wang, C. Yuan, J.X. Cheng, et al., Nat. Commun. 15 (2024) 758.
[15] X.X. Chen, R.Y. Wang, C.H. Cui, et al., Chem. Eng. J. 428 (2022) 131212.
[16] X.X. Chen, Q.Y. Zhong, S.J. Wang, et al., Acta Polym. Sin. 5 (2019) 469–484.
[17] C.H. Cui, X.J. Zhao, X.Y. Wang, et al., Polym. Chem. 16 (2025) 1595–1602.
[18] K.X. Chen, C.H. Cui, Z. Li, et al., ACS Macro Lett. 12 (2023) 543–548.
[19] H.X. Lei, S.N. Wang, D.J. Liaw, et al., ACS Macro Lett. 8 (2019) 582–587.
[20] W.Q. Ye, W.X. Fu, X.P. Liu, C. Yang, Z. Xu, Chin. Chem. Lett. 35 (2024) 108494.
[21] S.W. Feng, X.L. Peng, J.J. Cui, et al., Adv. Funct. Mater. 34 (2024) 2401431.
[22] H.G. Li, B. Zhang, H.T. Ye, et al., Sci. Adv. 10 (2024) eadl4387.
[23] F.Z. Wang, W.T. Gao, C.H. Li, Chin. Chem. Lett. 35 (2024) 109305.
[24] A. Inamdar, J. Cherukattu, A. Anand, B. Kandasubramanian, Ind. Eng. Chem. Res. 57 (2018) 4479–4504.
[25] C.F. Wang, Y.S. Tang, Y.X. Zhou, et al., Polym. Chem. 12 (2021) 3753–3761.
[26] Z.L. Cao, X.R. Xu, F.Y. Sun, et al., Adv. Funct. Mater. 35 (2025) 2505979.
[27] Z.P. Lei, H.X. Chen, C.Q. Luo, et al., Nat. Chem. 14 (2022) 1399–1404.
[28] Z.P. Lei, L.J. Wayment, J.R. Cahn, et al., J. Am. Chem. Soc. 144 (2022) 17737–17742.
[29] Y.A. Zhao, Z.Q.S. Cai, X.W. Qiu, et al., J. Mater. Sci. 59 (2024) 9350–9360.
[30] S. Chandrasekaran, E.B. Duoss, M.A. Worsley, J.P. Lewicki, J. Mater. Chem. A 6 (2018) 853–858.
[31] Z.X. Zhou, Y.W. Li, J. Zhong, et al., ACS Appl. Mater. Interfaces 12 (2020) 38682–38689.
[32] C.H. Cui, L. An, Z.L. Zhang, et al., Adv. Funct. Mater. 32 (2022) 2203720.
[33] C.H. Cui, X.X. Chen, L. Ma, et al., ACS Appl. Mater. Interfaces 12 (2020) 47975–47983.
[34] Q.J. Ma, L. Li, Y.F. Zhang, Y.P. Geng, J. Li, J. Funct. Polym. 37 (2024) 66–81.
[35] L. Pauling, Proc. Natl. Acad. Sci. U. S. A. 14 (1928) 359–362.
[36] L. Wu, Y.L. Song, Mater. Horiz. 12 (2025) 401–417.
[37] B. Zhang, H.G. Li, J.X. Cheng, et al., Adv. Mater. 33 (2021) 2101298.